The Company of **Biologists**

RESEARCH ARTICLE

HAND2-mediated epithelial maintenance and integrity in cardiac outflow tract morphogenesis

Meng Xia, Wen Luo, Hengwei Jin and Zhongzhou Yang*

ABSTRACT

During embryogenesis, epithelial organization is the prerequisite for organogenesis, in particular, for establishing the tubular structure. Recent studies provided hints about epithelial formation in early heart development, which has not been systemically explored. Here, we revealed a gradient of HAND2 protein in cardiac progenitors in the anterior dorsal pericardial wall (aDPW) and adjacent transition zone (TZ) in the outflow tract (OFT). Deletion of *Hand2* caused cell arrest and accumulation in the TZ, leading to defective morphogenesis. Although apicobasal cell polarity was unaffected, the key epithelial elements of adherens junction and cell-matrix adhesion were disrupted in the TZ of *Hand2* mutant mice, indicating poorly formed epithelium. RNA-seq analysis revealed altered regulation of the contractile fiber and actin cytoskeleton, which affected cardiomyocyte differentiation. Furthermore, we have identified *Stars* as being transcriptionally controlled by HAND2. STARS facilitates actin polymerization that is essential for anchoring the adhesive molecules to create cell adhesion. Thus, we have uncovered a new function of HAND2 in mediating epithelial maintenance and integrity in OFT morphogenesis. In addition, this study also provides insights for understanding cardiac progenitor contribution to OFT development.

INTRODUCTION

During embryogenesis, epithelial construction establishes the foundation for organogenesis, in particular, for establishing the tubular structure during the early stage of organ development (Kalluri and Weinberg, 2009; Nieto, 2013). The cardiac outflow tract (OFT) is a transient tubular structure that connects the main vasculature to cardiac ventricles. Morphogenesis of OFT is important for future septation of OFT into the trunks of aorta and pulmonary artery to establish the systemic and pulmonary circulation, which is required for the maintenance of physiology and survival (Harvey, 2002; Bruneau, 2008). In mice, the anterior second heart field (aSHF) progenitors from the splanchnic mesoderm (SpM) in the dorsal pericardial wall (DPW) migrate to the arterial poles of heart tube to form OFT and continue to facilitate its elongation and expansion for OFT morphogenesis (Black, 2007; Kelly et al., 2014). Perturbation of the OFT morphogenic process results in a spectrum of congenital

State Key Laboratory of Pharmaceutical Biotechnology, Department of Cardiology, Nanjing Drum Tower Hospital, The Affiliated Hospital of Nanjing University Medical School and MOE Key Laboratory of Model Animal for Disease Study, Model Animal Research Center, Nanjing University, Nanjing 210061, China.

*Author for correspondence (zhongzhouyang@nju.edu.cn)

Z.Y., 0000-0002-3272-5255

heart defects affecting OFT septation and alignment, which severely impairs cardiovascular function and compromises embryonic development and viability (Srivastava and Olson, 2000; Srivastava, 2006; Fahed et al., 2013).

Recently, several groups have recognized the epithelial properties of aSHF cardiac progenitors in the anterior DPW (aDPW) and adjacent transition zone (TZ) connecting the proximal OFT (TZ as the most distal OFT, Fig. 1A,B) (Cortes et al., 2018). For instance, it was reported that the Wnt5a-Disheveled (Dvl) planar cell polarity (PCP) signaling regulates epithelial conversion of the SHF progenitors in the SpM for cell deployment (Sinha et al., 2012; Li et al., 2016). This research also suggested that the core PCP gene *Vangl2* is involved in this process. A detailed and more refined analysis has since confirmed this possibility, demonstrating that Vangl2-regulated polarization is essential for epithelial establishment and cardiomyocyte differentiation in OFT morphogenesis; this also highlighted the relationship between cell polarity, the epithelial features of the distal OFT and differentiation of SHF progenitors to cardiomyocytes (Ramsbottom et al., 2014). Additionally, TBX1, a cardiac transcription factor required for OFT development, has been identified as a regulator of the epithelial properties of aSHF progenitors (Ramsbottom et al., 2014). These pioneering studies have defined a process of epithelial formation in OFT morphogenesis, whereby the cardiac progenitors with mesenchymal features in the aDPW constitute atypical apicobasally polarized epithelium that further develops into genuine epithelium in the adjacent, most distal, OFT, termed 'TZ', facilitating OFT morphogenesis.

Cell adhesive interactions, including adherens junctions (between cells) and cell-extracellular matrix (ECM) adhesion, are important elements of epithelial cells that help sustain tissue integrity in morphogenesis (Gumbiner, 2005; Takeichi, 2014). Adherens junctions are specialized structures that join together adjacent cells in the epithelium (Perez-Moreno et al., 2003). Two major adhesion molecules, E-cadherin and N-cadherin, are transmembrane proteins that bind epithelial cells together and, through their intracellular tails, connect to cytosolic α-, β- and γ-catenins (Thiery, 2003; Gumbiner, 2005). Furthermore, these catenins interact with the cytoskeleton of actin filaments and/or actomyosin bundles to achieve strong cell-cell adhesion (Parsons et al., 2010). By contrast, the epithelial cells also make contact with the ECM through membrane-localized integrins binding to matrix molecules, such as laminin and fibronectin (Hynes, 2002; Berrier and Yamada, 2007). Integrins further associate with the cytoskeleton of actin filaments and/or actomyosin bundles to result in stronger adhesion and/or help transmit signals from the extracellular environment to the cell. Therefore, actin filaments and/or actomyosin bundles have a crucial role in organizing cell adhesive interactions, the foundation for epithelial tissue formation (Parsons et al., 2010). Although these primary adhesive molecules have been characterized and described in the epithelium of aSHF progenitors in the DPW and TZ (Gumbiner, 2005; Takeichi, 2014), the regulators of these adhesion proteins remain unknown.

DEVELOPMENT

HAND2 is a key cardiac transcription factor essential for heart development, in particular for right ventricular (RV) formation (Srivastava et al., 1997; Yamagishi et al., 2000; Schindler et al., 2014; Vandusen et al., 2014). Although the roles of HAND2 in heart development and cardiomyocyte trans-differentiation have been extensively explored, the regulatory mechanisms exerted by HAND2 at molecular and cell biological levels in heart development remain less well understood. In zebrafish, Hand2 was found to be required for myocardial polarity in the early cardiac epithelium through negative modulation of fibronectin level, suggesting a role in tissue morphogenesis (Le and Stainier, 2004).

In this study, we investigated the regulation of OFT morphogenesis with an emphasis on the epithelial properties of the progenitors. We identified a gradient of HAND2 protein specifically in cardiac progenitors from aDPW and TZ epithelium. Deletion of *Hand2* in these progenitors caused abnormal cell arrest and accumulation at the TZ, hindering OFT morphogenesis. Although cell polarity was unaffected, adherens junction and cell-matrix adhesion was aberrant in the differentiating progenitors in the TZ of *Hand2* mutant mice. RNA-seq analysis also revealed disrupted regulation of the contractile fiber and actin cytoskeleton in *Hand2* mutant mice. Furthermore, we showed that *Stars* (*Abra*) is transcriptionally controlled by HAND2. STARS facilitates actin polymerization that is essential for cell adhesion formation. Thus, here we report a new role for HAND2 in mediating epithelial maintenance and integrity through regulation of actomyosin bundle assembly to construct cell adhesive interactions, which are crucial for OFT morphogenesis.

RESULTS

A specific gradient expression pattern of HAND2 protein occurs in aSHF progenitors of aDPW and TZ

OFT morphogenesis starts from embryonic day (E) 8.5-9.0 and then actively occurs between E9.5 and E10.5. During this period, OFT elongation and expansion occur through progressive addition of aSHF progenitors from the SpM to the distal OFT. To understand the regulation of OFT morphogenesis, we dissected distal OFT together with the aDPW, part of the SpM, from mouse embryos at E9.5 and E10.5 for gene expression profiling by RNA-seq analysis.

This analysis revealed the high level expression of several cardiac transcription factors, including *Nkx2-5*, *Hand2*, *Gata4*, *Hand1*, *Srf* and others (Fig. 1C). These results are consistent with previous studies from whole-mount *in situ* hybridization analyses (Prall et al., 2007; Ma et al., 2008; Vincentz et al., 2011). To better investigate the potential role of these genes in OFT morphogenesis, we generated specific monoclonal antibodies (in collaboration with Abcam), resulting in a HAND2-specific antibody worked successfully with immunofluorescence (IF) staining. Therefore, we performed a systematic study of HAND2 protein expression in early embryonic cardiovascular tissues.

At E8.0, HAND2 protein expression was found in both SpM and somatic mesoderm (SoM), where it largely overlapped with expression of Isl1 (Fig. 1D-K). At E8.5, high levels of HAND2 protein expression were observed in the aDPW, OFT and endocardium (Fig. 1L-O). At E9.5, high HAND2 protein expression was identified specifically in the aDPW, with more concentrated and intensive expression in the adjacent TZ, showing a gradient expression pattern (Fig. 1P-Q′). HAND2 accumulation peaked in the TZ at E9.5, after which its level declined, being then only found in a small number of cells in the RV. These results provide new information regarding the distribution of HAND2 in the cardiovascular tissues and suggest that

HAND2 has an important role in aSHF progenitors in the aDPW and TZ for OFT morphogenesis.

We also observed HAND2 expression in cardiovascular tissues from E10.5 to E15.5 (Fig. S1).

HAND2 regulates OFT morphogenesis

To test the possible involvement of HAND2 in OFT morphogenesis, we specifically deleted *Hand2* in aSHF progenitors using *Mef2c-AHF*-Cre-mediated ablation (Verzi et al., 2005). IF staining for HAND2 showed successful deletion of *Hand2* in aSHF progenitors (Fig. 2A-D). *Hand2* mutant mice (*Hand2^f/f^*; *Mef2c-Cre*) displayed substantially smaller OFT and RV compared with controls (Fig. 2E-F′). Given that this RV phenotype has been intensively investigated elsewhere (Tsuchihashi et al., 2011), we focused our study on OFT morphogenesis.

Intriguingly, histological analysis revealed multiple layers of cells in the distal OFT of *Hand2* mutant mice, whereas, in the OFT of control mice, there were only one or two layers of cells (Fig. 2G-G′,I-I′). Detailed analysis showed up to four or five layers of cells in the distal OFT in *Hand2* mutant embryos compared with one or two layers of cells in control embryos (Fig. 2H,J). This change in cell layers occurred in the distal OFT but not in the aDPW, although *Hand2* was also deleted in the aDPW (Fig. S2A,B). *Rosa26-mTmG* reporter mice have cell membrane-localized green fluorescent protein (GFP) and red fluorescent protein (RFP) that can precisely outline the shape of cells. Therefore, we used these mice to study OFT wall thickness, with horizontal sections of the distal OFT further confirming the multiple layers of cells in *Hand2* mutant mice (Fig. 2K,L). Quantification of the distal OFT wall thickness also demonstrated substantially increased OFT thickness in *Hand2* mutant mice (Fig. 2M). We also used the *Rosa26-mTmG* reporter line to reveal differences in the morphology of OFT cells in the *Hand2* mutant versus control mice (Fig. 2N-Q). Cell circularity analysis further revealed the profoundly reduced roundness of OFT cells in *Hand2* mutant mice compared with controls (Fig. 2R).

Taken together, these results demonstrated defective OFT morphogenesis and cell accumulation in the distal OFT of *Hand2* mutant mice.

aSHF progenitors are arrested in the TZ of *Hand2* mutant mice

To understand the cause of cell accumulation in the distal OFT of *Hand2* mutant mice, we examined cell proliferation and survival. Previous work showed that enhanced thymoma viral proto-oncogene 1 (Akt) signaling in aSHF progenitors promotes cell proliferation in the caudal SpM, the increased progenitor pool of which can be visualized directly by using a GFP reporter mouse line at E9.5 (Luo et al., 2015). Thus, we used this strategy to examine the progenitor pool in *Hand2* mutant and control mice at E9.5. The results showed little difference between the two groups at both E9.5 (Fig. S3A,B) and E10.5 (Fig. S3C,D). We then performed IF staining to study KI67^{+} (Mki67^{+}) and Isl1^{+} cells at E9.5, and showed that the number of Isl1^{+} cells and the percentage of KI67^{+}/Isl1^{+} cells in aDPW were comparable between *Hand2* mutant and control mice (data not shown). Further IF staining for phosphohistone H3 (pHH3)[+] at E9.5 obtained similar results (Fig. S3E-G). IF staining for pHH3^{+} cells in the OFT failed to detect a difference between the two groups (Fig. S3H-J). In addition, terminal deoxynucleotidyl transferase dUTP nick end labeling (TUNEL) staining to examine cell apoptosis indicated no difference between *Hand2* mutant and control mice (Fig. S3K-M).
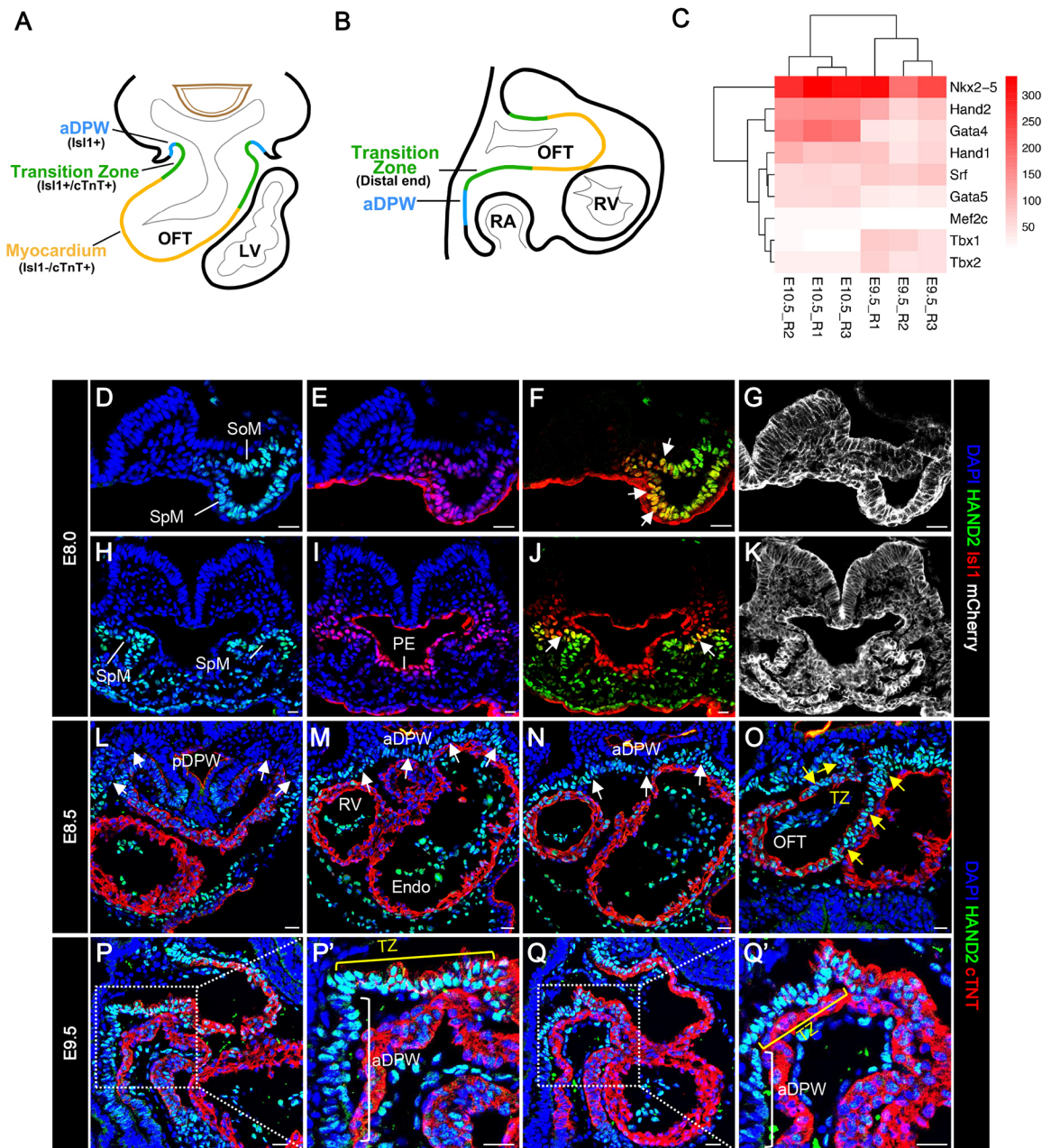
Fig. 1. Expression pattern of HAND2 in early mouse embryos. (A,B) Schematics showing the early cardiac structures of E9.5 mouse embryos as transverse (A) and sagittal (B) sections. (C) Heatmap showing the expression level of genes encoding key cardiac transcription factors in the aDPW and OFT at E9.5 and E10.5. (D-K) HAND2/Isl1 staining of sections from E8.0 mouse embryos. The cell membrane is labeled with mCherry. HAND2/Isl1 double-positive nuclei are shown in yellow (indicated by arrows) and located in lateral plate mesoderm, including SpM and SoM in F and J, respectively. (L-Q′) HAND2/cTNT staining at E8.5 and E9.5. P′ and Q′ are higher magnifications of the boxed areas in P and Q, respectively. White arrows and square brackets indicate the pDPW and aDPW regions, whereas yellow arrows and square brackets mark the TZ. Although cells in the aDPW showed modest HAND2 protein expression, those in the TZ showed higher expression levels (P′,Q′). Endo, endocardium; LV, left ventricle; pDPW, posterior dorsal pericardial wall; PE, pharyngeal endoderm; RA, right atrium. Scale bars: 50 μm.

Collectively, these studies demonstrated unchanged cell proliferation and survival in aSHF progenitors of *Hand2* mutant mice, indicating that cell proliferation and apoptosis do not account for the defective OFT morphogenesis in these mice.

OFT morphogenesis relies on the addition (i.e. movement and/or migration) of aSHF progenitors to the distal OFT during E9.5-10.5 (Kelly et al., 2014). Therefore, we examined the movement and/or migration of aSHF progenitor cells into OFT. The primary characteristics of aSHF progenitors are robust cell proliferation but delayed cell differentiation, which contribute to the elongation and expansion of the OFT (Vincent and Buckingham, 2010). By IF staining for Isl1$^+$ cells, we first examined the number of aSHF progenitors deployed in the OFT and showed that, whereas the total cell number was comparable between *Hand2* mutant and control mice at both E9.5 and E10.5, the distribution pattern differed between the two groups. In the control mice, Isl1$^+$ cells lined the whole OFT; by contrast, they cumulated in the TZ in *Hand2* mutant mice (Fig. 3A-F).

We also performed 5-ethynyl-2'-deoxyuridine (EdU) pulse-chase assays to trace the movement and/or migration of aSHF
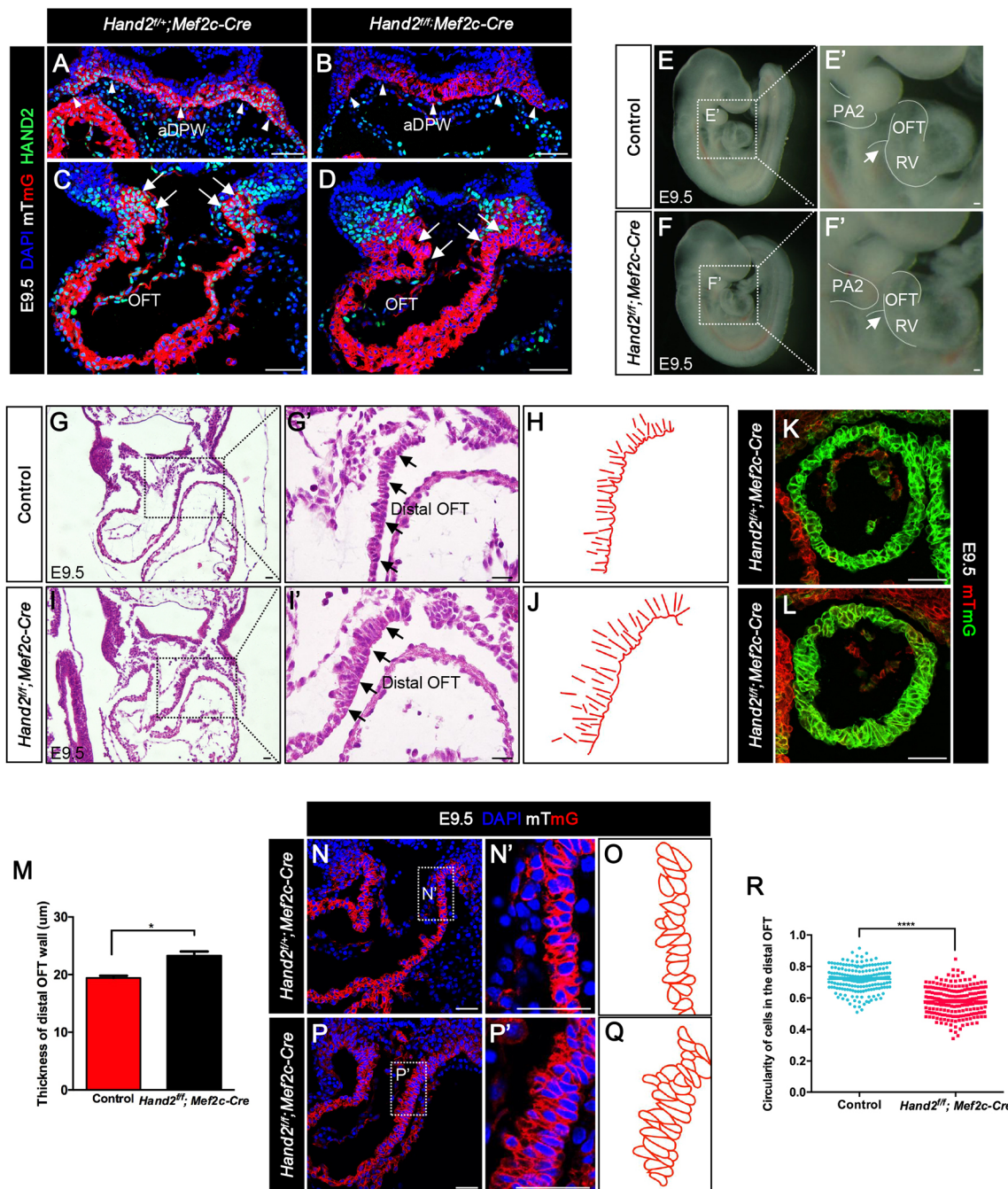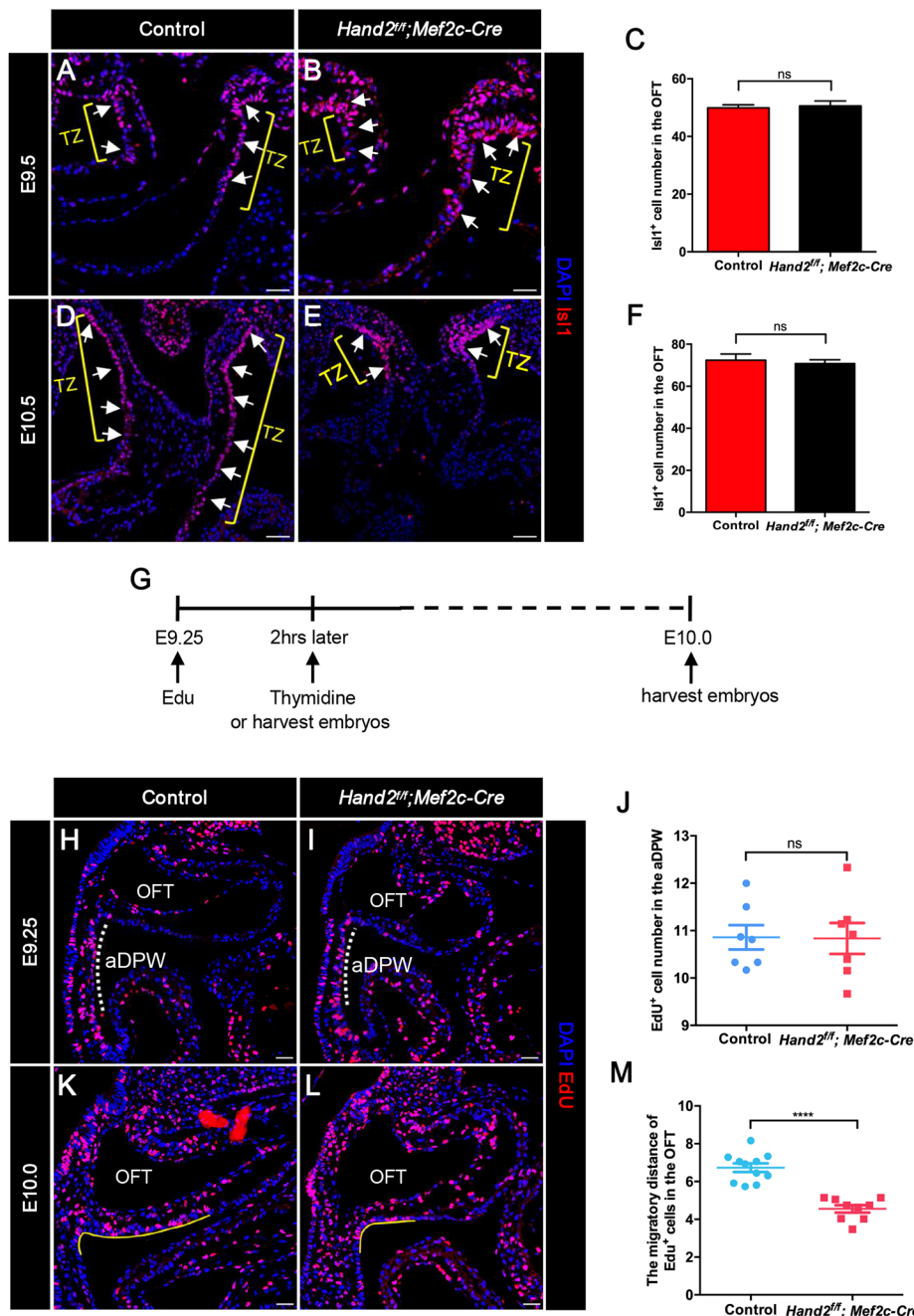
Fig. 2. Histological and IF staining analysis of the outflow tracts. (A-D) IF staining for HAND2 shows that the protein was absent in the aDPW (indicated by arrowheads in A and B) and TZ (indicated by arrows in C and D) of *Hand2* mutant mice. The OFT was smaller in *Hand2* mutant mice (D) than in control mice (C). (E-F′) Gross analysis of embryos at E9.5. E′ and F′ are higher magnifications of the boxed areas in E and F, respectively. The OFT and RV were significantly reduced in the *Hand2* mutant mice (indicated by arrows). PA2, second pharyngeal arch. (G-J) Histological analysis of transverse sections of OFT at E9.5. G′ and I′ are higher magnifications of the distal OFT in the boxed areas in G and I, respectively. H and J are schematics of the cell layers in the distal OFT wall referring to G′ and I′, respectively. The arrows indicate distal OFT. The lines represent the long axis of individual cells. (K,L) Cross-sections of OFT from control (*Hand2^f/+^*; *Mef2c-Cre*; mTmG) and *Hand2* mutant (*Hand2^f/f^*; *Mef2c-Cre*; mTmG) embryos, respectively. (M) Quantification of the thickness of distal OFT wall in K and L (seven serial sections per embryo from three control and three *Hand2* mutant embryos were analyzed). (N-Q) Transverse sections of control (*Hand2^f/+^*; *Mef2c-Cre*; mTmG) and *Hand2* mutant mice (*Hand2^f/f^*; *Mef2c-Cre*; mTmG) embryos. N′ and P′ are higher magnifications of the boxed areas in N and P, respectively. O and Q show the cell morphology in N′ and P′, respectively. (R) Scatter plot showing the decreased circularity of stacked cells in *Hand2* mutant embryos (*n*=183 cells from five control embryos and *n*=202 cells from five *Hand2* mutant embryos). All data are mean±s.e.m. *P<0.05, ****P<0.001. Scale bars: 50 μm.

progenitors towards the distal OFT. A large dose of EdU was administrated to embryos at E9.25, followed by thymidine administration 2 h later to compete against EdU incorporation (Fig. 3G). Continuous and similar numbers of EdU-labeled

progenitors in the aDPW were found between the two groups at E9.25 (Fig. 3H-J). However, the assays at E10.0 revealed a markedly reduced distance of cell movement and/or migration in *Hand2* mutant compared with control mice (Fig. 3K-M).

Fig. 3. IF staining analysis of cardiac progenitors and EdU pulse-chase assay. (A-F) IF staining for Isl1 in transverse sections from embryos at E9.5 and E10.5. The number of Isl1-positive aSHF progenitors in TZ (arrows) are quantified in C and F (five to six serial sections per embryo from three control and three *Hand2* mutant embryos). (G) Schematic diagram showing the time points for the EdU pulse-chase assay. (H,I,K,L) EdU staining in sagittal sections from control and *Hand2* mutant embryos at E9.25 and E10.0. The regions of highly proliferating progenitors in the aDPW are marked with a white dotted line in H and I. The migratory distances in OFT are indicated by yellow lines in K and L. (J,M) Scatter plots showing quantification of the number of EdU-positive cells in the aDPW at E9.25 (9-18 serial sections per embryo from seven control and seven *Hand2* mutant embryos) and cell migratory distance in OFT at E10.0 (5-15 serial sections per embryo from 11 control and nine *Hand2* mutant embryos), respectively. All data are mean±s.e.m. ns, not significant. ****$P<0.001$. Scale bars: 50 μm.

Taken together, these results indicate that the cell arrest of aSHF progenitors at the TZ is the primary cause of defective OFT morphogenesis in *Hand2* mutant mice.

HAND2 deficiency causes disrupted cell adhesion in the TZ

Recent studies have recognized the epithelial properties of aDPW and adjacent TZ, which primarily comprise aSHF cardiac progenitors (Francou et al., 2014; Ramsbottom et al., 2014). To understand the causes of cell arrest of aSHF progenitors at the distal OFT at the cell biology level, we investigated the epithelial features in both aDPW and TZ.

One epithelial property is cell polarity. IF staining for ZO-1 (tight junction protein 1; Tjp1) and atypical protein kinase C, zeta [aPKCζ (Prkcz)] showed comparable patterns in the aDPW and TZ between *Hand2* mutant and control mice at E9.5, indicating normal cell polarity (Fig. 4A-D′). By contrast, when another epithelial feature, adherens junctions, was examined through IF staining for the two essential adhesive molecules of N-cadherin and E-cadherin, it demonstrated a severely disrupted pattern in the TZ of *Hand2* mutant compared with control mice (Fig. 4E-H). Interestingly, the protein levels of both N-cadherin and E-cadherin were unaltered in OFT tissues via western blot analysis in *Hand2* mutant mice compared with controls (Fig. S4A). We also studied α- and β-catenin by IF staining and failed to detect an obvious difference between the two groups (Fig. S4B-E″).

Next, we investigated another type of cell adhesion, cell-matrix adhesion, in these areas. The ECM protein fibronectin was normally distributed in *Hand2* mutants (Fig. 5A-D). However, another ECM protein, laminin, showed both apical and basal distribution in TZ of *Hand2* mutant embryos compared with a
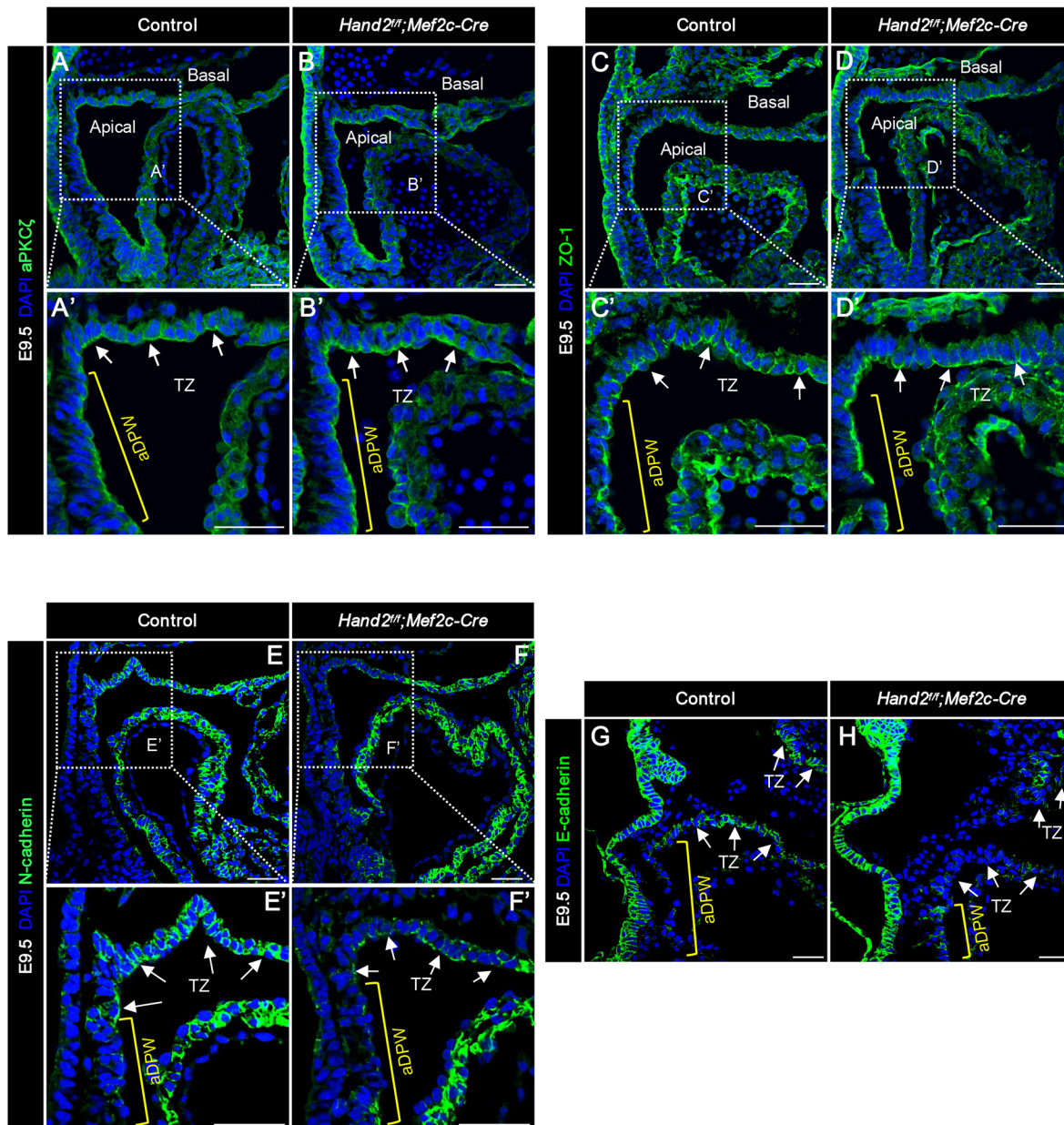
Fig. 4. IF staining analysis to analyze cell polarity and cell adhesion. (A-B′) IF staining for aPKCζ showing apical membrane location in aDPW (indicated by yellow square brackets) and TZ (indicated by white arrows) at E9.5. A′ and B′ are higher magnification of the boxed areas in A and B, respectively. (C-D′) IF staining for ZO-1 showing localization at the apical membrane in aDPW (indicated by yellow square brackets) and TZ (indicated by white arrows) at E9.5. C′ and D′ are higher magnifications of the boxed areas in C and D, respectively. Both control and *Hand2* mutant embryos manifest similar patterns of aPKCζ and ZO-1 staining in the aDPW and TZ. (E,F) IF staining for N-cadherin in sagittal sections at E9.5. E′ and F′ are higher magnifications of boxed areas in E and F, respectively. Levels of N-cadherin gradually increase from aDPW to TZ, and its intercellular distribution is evident in control mice. By contrast, its expression level and distribution are substantially altered in the TZ of *Hand2* mutant mice. (G,H) IF staining for E-cadherin. A similar pattern to N-cadherin is observed in control mice, whereas it is disrupted in the *Hand2* mutant mice. White arrows indicate TZ and yellow square brackets indicate aDPW. Scale bars: 50 μm.

predominantly basal location in controls (Fig. 5E,F). Other important molecules involved in cell-matrix adhesion, namely integrin β1 (ITGB1), vinculiln and ILK, all displayed severely attenuated intensity, particularly in the lateral interfaces between cells of the TZ in *Hand2* mutant mice compared with controls (Fig. 5G-L″).

In addition, the cytoskeleton of actin filaments and actomyosin bundles that associate with adhesive molecules in both adherens junction and cell-matrix adhesion, showed remarkably altered patterns in *Hand2* mutant mice. Phalloidin staining for F-actin demonstrated obvious attenuated actin filaments in the tissue of TZ in *Hand2* mutant mice (Fig. 6A-B″). Compared with controls, the signal in the basal side of the TZ was weaker and was almost completely lost in the lateral side in mutant mice. We also detected an increase in monomeric G-actin levels in the distal OFT of *Hand2* mutant mice (Fig. 6C-G), suggesting weakened actin polymerization or excessive depolymerization. Consistent with the change in actin filaments, investigation of the patterns of associated nonmuscle myosin II (NMMIIB) together with its regulator, RMLC (active form of p-RMLC, p-Ser19), revealed nearly identical
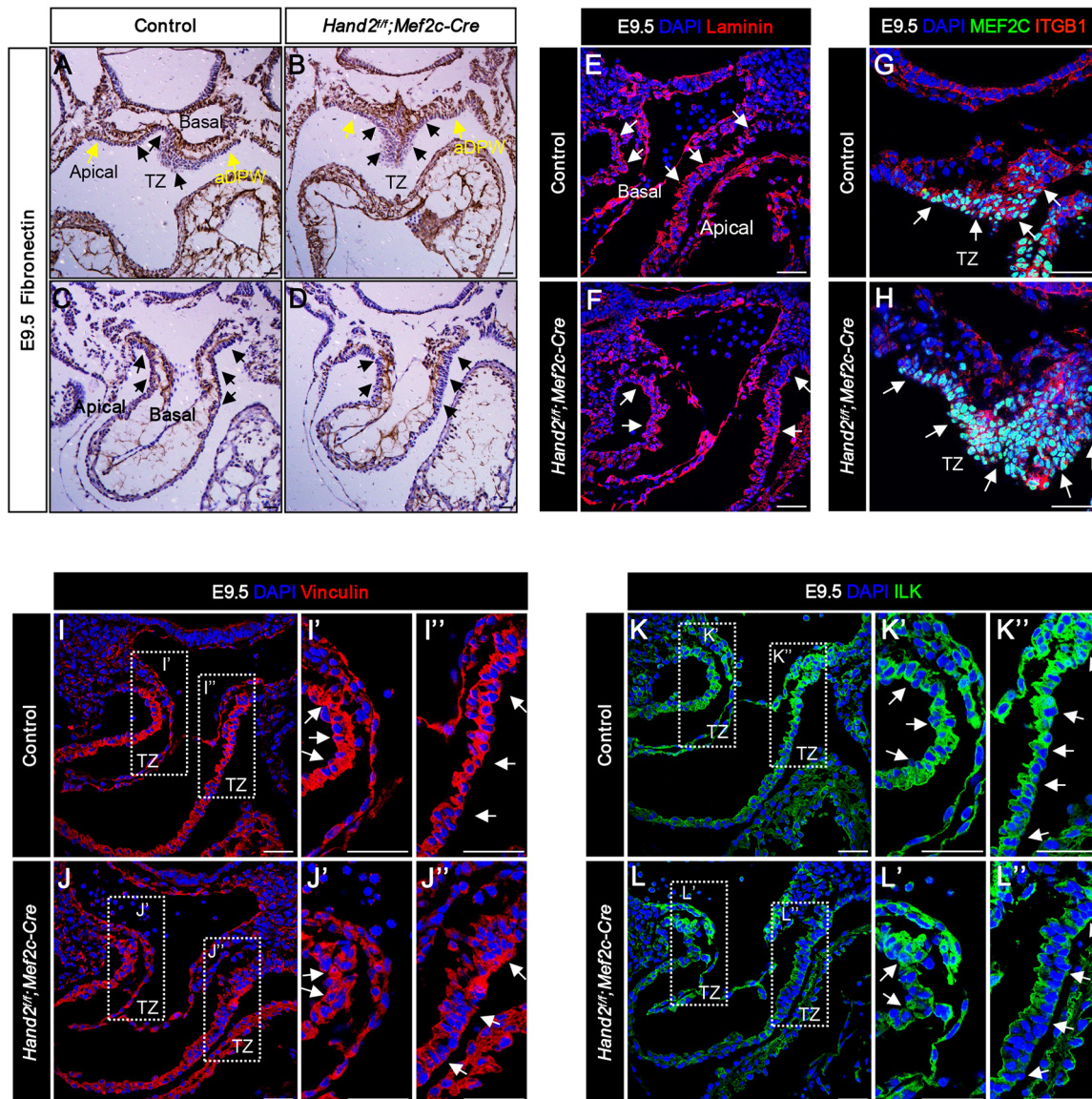
DEVELOPMENT

6

Fig. 5. Immunohistological and IF staining analysis. (A-D) IF staining for fibronectin in E9.5 transverse sections revealed it at the basal side from aDPW (indicated by yellow arrows) throughout the whole TZ (indicated by black arrows), with similar patterns in control and *Hand2* mutant embryos. (E,F) IF staining for laminin. A clear and predominantly basal distribution of laminin was observed in the TZ (indicated by arrows) in control embryos in contrast to an equal distribution at both the apical and basal sides (indicated by arrows) in *Hand2* mutant embryos. (G,H) IF staining for IGBT1 and Mef2c in the TZ (similar to cTNT staining). IGBT1 shows principally basal and lateral membrane localization, but to a lesser intensity at the apical side of TZ in control mice, whereas its level is decreased in *Hand2* mutants. (I-J″) IF staining for vinculin and (K-L″) for ILK. Compared with controls, the lateral cellular distribution (between cells) of both vinculin and ILK are abolished in the mutant mice at E9.5. I′-L″ are higher magnifications of boxed areas in I-L. The arrows in I-L indicate TZ area. Scale bars: 50 μm.

changes to those of actin filaments (Fig. 6H-K; Fig. S5A-F). Staining of Phalloidin and p-RMLC in the aDPW showed comparable patterns between control and *Hand2* mutant mice (Fig. S5G-J).

Collectively, these data reveal severely disrupted cell adhesion in the TZ in *Hand2* mutant mice: although HAND2 was not needed for cell polarity establishment, it was required for the formation of cell adhesions.

Deletion of *Hand2* alters the expression of the genes involved in the actomyosin network

To understand the molecular regulation of cell adhesion in the progenitors of TZ, we collected tissue from aDPW and OFT at ~E9.0-E9.5 for RNA-seq analysis. Heatmaps showed that, compared with controls, most genes were downregulated in *Hand2* mutant mice, suggesting a role for HAND2 in activating gene transcription (Fig. 7A). Gene Ontology (GO) analysis revealed that the genes with significantly reduced expression level were within the contractile fiber and actin cytoskeleton catalogs (Fig. 7B). RT-quantitative (q)PCR analysis confirmed the changes of several genes (Fig. S6A). The RNA-seq data (Fig. 7A) revealed a substantial reduction in the expression of *Stars* (Akiko et al., 2002; Koichiro et al., 2005), a conserved actin-binding protein that facilitates actin polymerization. We verified this change by RT-qPCR (Fig. 7C). IF staining demonstrated a near-complete loss of STARS throughout the OFT of *Hand2* mutant mice (Fig. 7D,E). Western blotting analysis also confirmed this change (Fig. S6B).
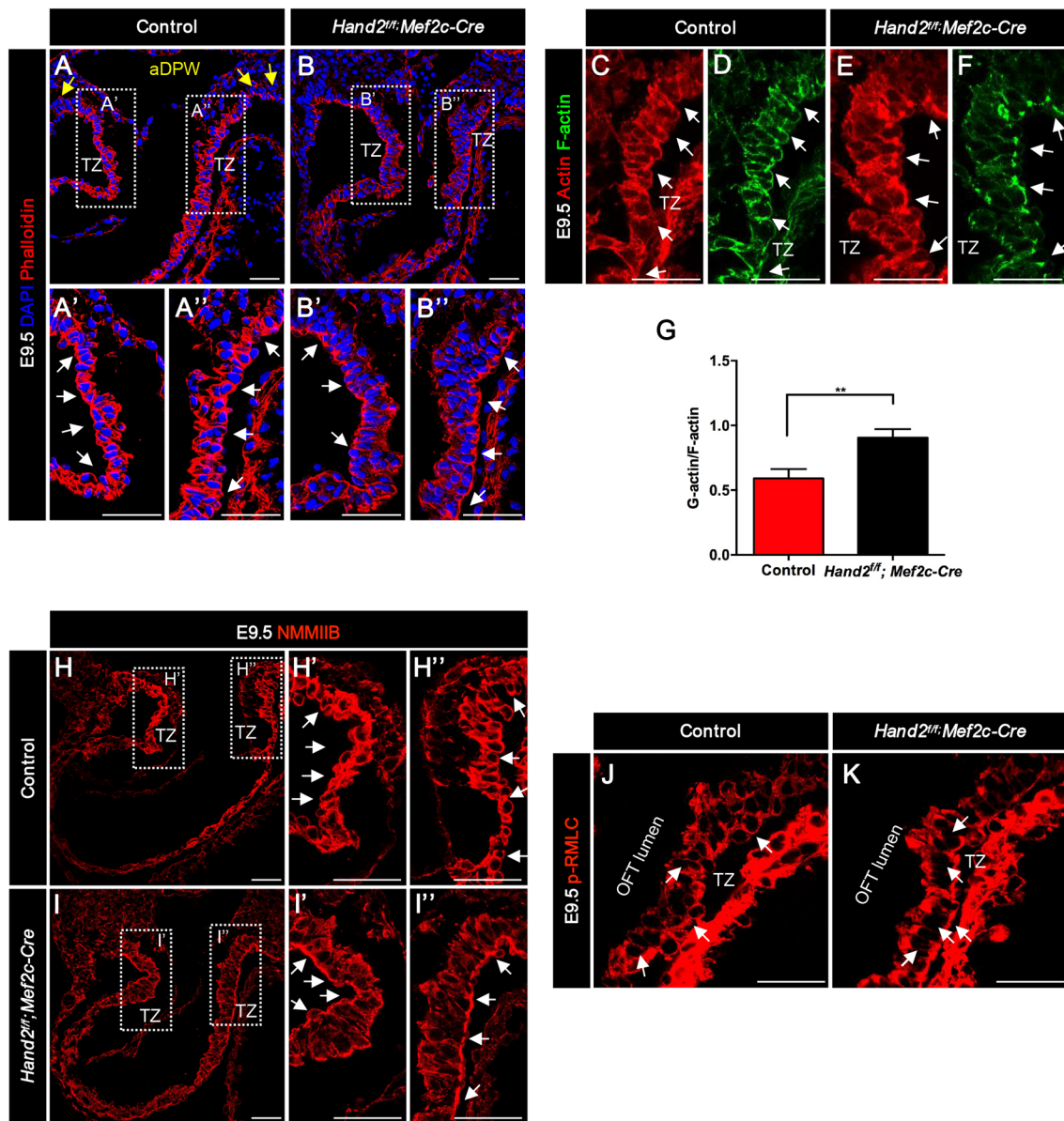
Fig. 6. Study of actin cytoskeleton and associated nonmuscle myosin architecture. (A-B″) Phalloidin IF staining. A′ and B″ are higher magnifications of the boxed areas in A and B, respectively. Compared with controls, where the signal is strong in both the apical and basal sides together with the lateral surfaces (indicated by arrows), the mutant mice generally show weak intensity, with some apical signals between neighbors in the TZ (indicated by arrows). Yellow arrows indicate aDPW and white arrows indicate TZ area. (C-G) Total actin and Phalloidin (F-actin) co-immunostaining to measure the ratio of monomer form actin (G-actin) to filamentous actin (F-actin) in the TZ. (G) The scatter plot shows quantification from C-G (three serial sections per embryo from six control and six *Hand2* mutant embryos). Data are mean±s.e.m. *$P<0.05$. (H-I″) IF staining for NMMIIB in the TZ. H′, H″, I′ and I″ are higher magnifications of the boxed areas in H and I. A similar altered pattern in NMMIIB staining to that for F-actin staining is observed in the mutant mice (indicated by arrows). (J,K) IF staining for p-RMLC in the TZ at E9.5. Scale bars: 50 µm.

We also examined the levels of differentiation markers of cardiomyocytes in control and *Hand2* mutant mice at E9.5. The expression levels of *Nkx2.5*, *Mef2c* and *Gata4*, together with those of their proteins, were comparable between the two groups (Fig. S6C-I). Next, we performed IF staining for cTNT (troponin T2, cardiac; Tnnt2) and α-actinin (key components of the sarcomere apparatus) to check cardiomyocyte maturation in the TZ. The results revealed profoundly reduced protein levels together with aberrant localization patterns in cardiomyocytes of *Hand2* mutant mice (Fig. S6J-M) indicating cardiomyocyte differentiation defects. The expression levels of *Tnnt2* and *Actn2* (encoding α-actinin) were also significantly reduced in *Hand2* mutant mice (Fig. S6A).

Identification of *Stars* as the direct downstream target gene of HAND2

The above data suggested that HAND2 directly activates the transcription of *Stars*. Therefore, we explored the relationship between HAND2 and *Stars*. HAND2 is a member of the Twist family of basic helix-loop-helix (bHLH) transcription factors and binds the consensus elements termed E-boxes (CANNTG) or degenerate sequences of D-boxes (CGNNTG) as either homodimers or heterodimers, to activate the transcription of downstream genes (Firulli et al., 2003). Through bioinformatics analysis, three well-conserved E-boxes were identified located upstream of the mouse *Stars* transcription start site (TSS) (Fig. 7F).
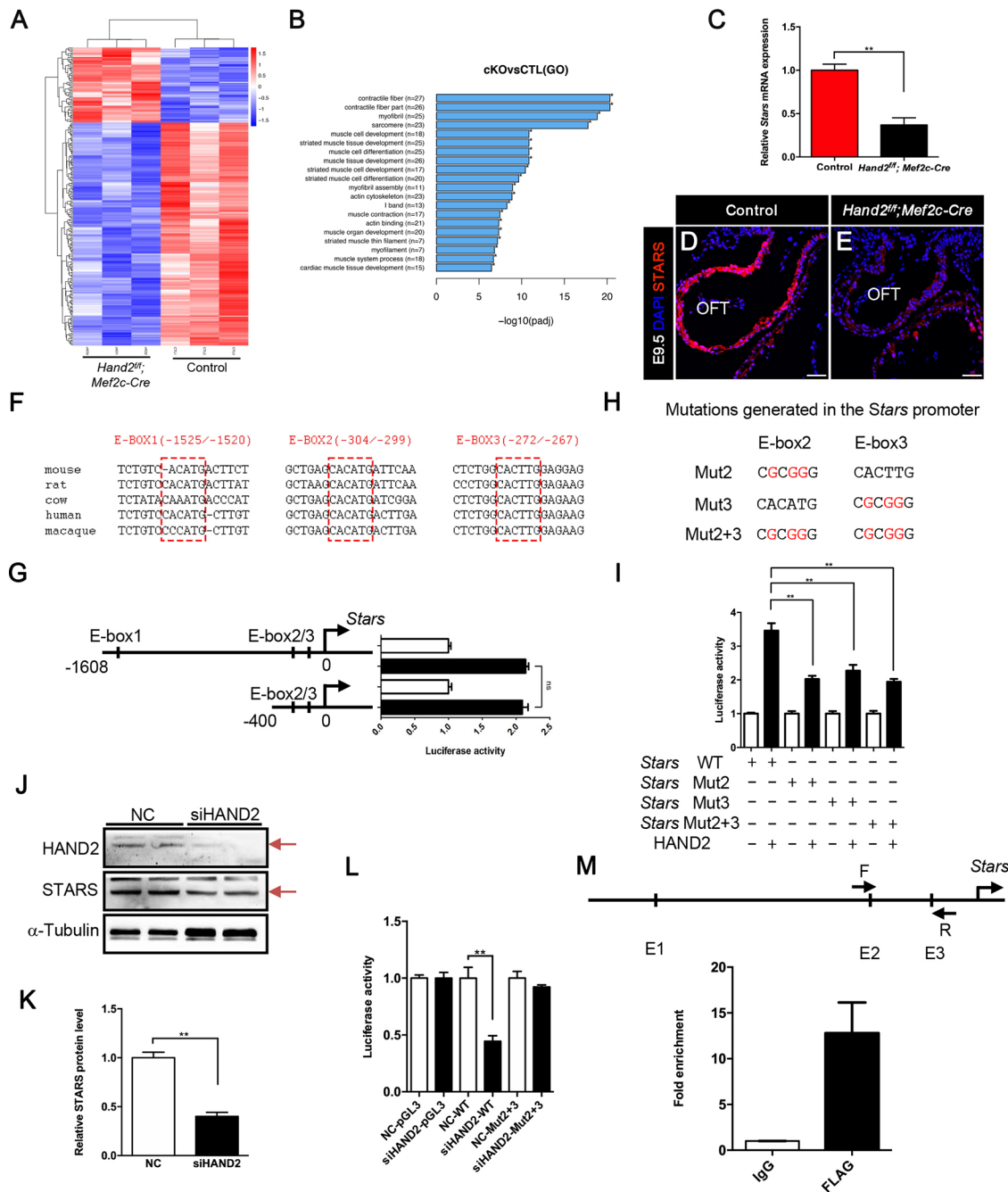
Fig. 7. Transcriptome analysis and characterization of *Stars* as a direct target gene of HAND2. (A) Heatmap of differentially expressed genes between control and *Hand2* mutant mice. A total of 250 genes, 187 of which with decreased and 63 with increased expression levels, are significantly altered in *Hand2* mutant embryos [fold change (FC) >1.3, false discovery rate (FDR) <0.05]. (B) GO enrichment showing that differentially expressed genes are enriched for pathways linked to contractile fibers and the actin cytoskeleton. (C) qPCR measurement of *Stars* expression level in the OFT at E9.5. (D,E) IF staining for STARS, showing a significantly reduced protein level in the whole OFT in *Hand2* mutant embryos. (F) Three well-conserved E-boxes are located upstream of the mouse *Stars* TSS via comparative sequence analysis. (G) Luciferase reporter assay in 293T. (H) Mutation sites for the two E-boxes. (I) Luciferase reporter assay in HEK293T cells. (J) Western blot analysis of STARS protein level in NC and siHAND2 H9C2 cells. (K) Quantification of J showing decreased STARS protein level. (L) Luciferase reporter assay in H9C2 cells. (M) ChIP assay performed in H9C2 cells showing direct HAND2-binding site between the E2 and E3 located upstream of the rat *Stars* TSS. Scale bars: 50 μm.

To test whether exogenous HAND2 impacts the *Stars* promoter, we cloned the 1608-bp and 400-bp fragments upstream of the *Stars* TSS to PGL3-basic plasmids for luciferase reporter assays. The results showed that the 400-bp fragment could be activated by HAND2 (Fig. 7G). Next, we generated mutation constructs to abolish the E-box sequences of E2 and E3, with both mutants showing strongly reduced reporter activity in response to HAND2,

suggesting that these two E-boxes are responsible for transcriptional regulation by HAND2 (Fig. 7H,I). The combined double mutations of E2 and E3 showed a similar effect as the single mutation of E2, suggesting the more important role of E2 in this regulation (Fig. 7I).

Furthermore, we investigated the regulatory relationship between endogenous HAND2 and STARS in H9C2 rat cardiomyocyte-like cells. Knockdown of *Hand2* significantly reduced STARS levels, as

revealed by western blot analysis (Fig. 7J,K), and also profoundly reduced luciferase reporter activity (Fig. 7L). Finally, chromatin immunoprecipitation (ChIP) studies confirmed that HAND2 directly binds to *Stars* (Fig. 7M).

Taken together, these data demonstrated that HAND2 directly regulates *Stars* expression. STARS also controls an intracellular signaling cascade to stimulate the MRTF-SRF transcriptional pathway. The SRF protein level in the OFT was normal (Fig. S7A-C), and the MRTF-A pattern in the TZ was unchanged (Fig. S7D-E′) in *Hand2* mutant mice.

Collectively, these results are consistent with the results of, and support the conclusions made by, Métais and colleagues in their study (Métais et al., 2018), suggesting the important role of actin cytoskeleton organization and remodeling in cardiomyocyte differentiation in the TZ.

DISCUSSION

In this study, we characterized the epithelial features of the aDPW and TZ in early mouse embryos by investigating alterations in these tissues in *Hand2* mutant mice, providing additional understanding of the new role for the cardiac-specific transcription factor HAND2 in mediating epithelial maintenance and integrity for OFT morphogenesis.

The HAND2-specific antibody enabled us to observe a specific gradient expression pattern in the aDPW and TZ. Removal of *Hand2* from these areas disrupted cell adhesion, including adherens junction and cell-matrix adhesions. Mechanistically, HAND2 regulates the expression of the actin and myosin cytoskeleton together with their regulators to establish cell adhesions for epithelial formation in the TZ, facilitating OFT morphogenesis.

The epithelial behavior of the aDPW and TZ has only recently been recognized through research that has provided a foundation for understanding the regulatory signaling pathways involved in the developing cardiac epithelium and the principles for establishing cell polarity. However, understanding of this paradigm of epithelial structure has been limited to the fact that Wnt5a-Dvl PCP signaling is necessary to facilitate epithelial formation, whereas PKC, TBX1 and Vangl2 are responsible for cell polarity establishment in these areas.

Our study demonstrates a new role for HAND2 in maintaining the epithelial integrity in OFT morphogenesis, and we propose a model based on this study (Fig. S8A,B). Our results also help us to understand the contribution of SHF progenitors to the OFT. For more than a decade, it has been well accepted that these progenitors move and/or migrate into the OFT, although the mechanisms involved have been unclear. Our study demonstrated that, by organizing epithelial tissue, SHF progenitors contribute to the OFT and that HAND2 has a pivotal role in maintaining the epithelial integrity. Consequently, the OFT morphogenic process can be understood from a new perspective, whereby the epithelium is continuously generated in the TZ, which pushes the caudal extension of the coherent epithelial sheet of primary OFT (Fig. S8A), a process similar to the involution of mesoderm and endoderm movement during in *Xenopus* gastrulation (Wolpert et al., 2006).

Our results also identified a new role of HAND2 in regulating cell adhesions and shed light on the underlying mechanisms. By transcriptionally regulating the expression of actomyosin cytoskeleton genes and their regulators, HAND2 is crucially involved in the construction of the cell adhesions in the cardiac epithelium and also maintains the epithelial integrity. Our results also suggest that the HAND2-regulatory actin cytoskeleton is required for correct cellular distribution and stability of N- and E-cadherin. Recently, Chien and colleagues reported N-cadherin-mediated cell proliferation and differentiation in the second heart

field through systemic investigation of SHF-specific N-cadherin-deficient mice (Boon-Seng et al., 2014). Their results pinpoint the importance of N-cadherin in regulating SHF development and OFT morphogenesis.

Analysis of the RNA-seq data identified *Stars* as one of the most downregulated genes in *Hand2* mutant mice. Previous studies revealed STARS to be actin-binding protein facilitating actin polymerization (Koichiro et al., 2005). Therefore, we investigated whether *Stars* is a direct transcriptional target of HAND2 through a series of biochemical analysis and *in vivo* immune-staining studies, which demonstrated *Stars* to be a downstream effector of HAND2. A recent study reported defective heart development in zebrafish with knocked down *stars*, indicating a crucial function of STARS in heart formation (Chong et al., 2012). Although *Stars* mutant mice are viable, this does not contradict our mechanistic conclusions. A panel of genes encoding distinct types of actin, such as *Actc1* and *Acta2*, showed significant reduction in expression levels in *Hand2* mutant mice. Actin molecules are materials for actin filament assembly to establish the actin cytoskeleton and STARS promotes this process. In *Hand2* mutant mice, both actin materials and their assembly regulator, STARS, were reduced significantly. Therefore, the actin cytoskeleton defects are a combinatory effect of reduced actin and STARS.

The HAND2-regulatory actomyosin filament formation and STARS-mediated actin polymerization are also involved in the myofibril assembly in the cardiomyocytes. We observed a disrupted sarcomere structure in the RV of *Hand2* mutant mice, which might account for the heart failure that leads to embryonic lethality by E13.5. How HAND2 couples the regulation of actin cytoskeleton together with that of actin-based sarcomere assembly is well understood. However, the regulatory mechanisms of actin-sarcomere assembly are more complex and require further detailed investigations.

Our study also defines a role of mammalian HAND2 that is distinct from its zebrafish counterpart in establishing cardiac epithelial organization. Zebrafish HAND2 is uniquely required for cell polarity of the early myocardial epithelium, whereas we identified a new function of mammalian HAND2 in cell adhesions.

Srivastava was one of the first to generate *Hand2* (*dHAND*) global null mice for delineating HAND2 function in heart development, leading to the seminal discovery of HAND2 involvement in early heart formation (Srivastava et al., 1997). Recent research by his group using single cell transcriptome analyses revealed HAND2 to regulate OFT myocardial specification (De Soysa et al., 2018 preprint). This is consistent with our results and provides further insights into SHF progenitor cell fate and differentiation.

A recent report suggests the involvement of a Wnt5 signaling cascade in regulating actin polymerization (Li et al., 2016). In combination with our study, it is possible that HAND2 functions downstream of Wnt5a signaling to control actin filament and/or bundle formation.

In summary, we have revealed an important role for HAND2 in mediating cell adhesion by maintaining epithelial integrity, which is crucial for OFT morphogenesis. We believe that this study will help researchers to understand further the pathogenesis of certain congenital heart defects.

MATERIALS AND METHODS
Mice
The following mouse strains were used in this study: *Hand2* floxed mice (Holler et al., 2010), *Mef2c-AHF-Cre* mice (Verzi et al., 2005) and *Rosa26-mTmG* mice (from the Jackson Laboratory, Stock No. 023035). All these mouse lines were previously reported. The experimental animal facility has

been accredited by the Association for Assessment and Accreditation of Laboratory Animal Care International (AAALAC); the Institutional Animal Care and Use Committee (IACUC) of Model Animal Research Center of Nanjing University, China, approved all the animal protocols used in this study.

Generation of HAND2 antibodies
HAND2 antibodies were generated as a collaborative project with Abcam (R&D Center, Hangzhou, China). We first tested the specificity of the antibody product using cell transfection and *Hand2*-knockout tissues. We obtained a good batch of rabbit monoclonal antibody that is suitable for both IF staining and western blotting analysis. Abcam provided a portion of this product without charge, but it is now on the market with the catalog number of Ab200040.

Histology, immunofluorescence and immunohistochemistry
Mouse embryos were fixed in 4% PFA for 2 h, dehydrated, embedded in paraffin or in optimal cutting temperature compound (OCT), and then sectioned. Histological sections were stained with Hematoxylin and Eosin (H&E) or used for TUNEL, IF and immunohistochemical (IHC) analysis. IF and IHC were carried out using standard procedures (Xiao et al., 2017). Embryos were fixed in 4% PFA, then rinsed in PBS and incubated in 30% sucrose at 4°C until sinking. The embryos were then embedded in OCT medium and snap-frozen in liquid nitrogen and stored at −80°C. Sections were cut at a thickness of 8 μm. Detailed information on the primary antibodies and dilutions is provided in Table S1. Fluorescent secondary antibodies were obtained from Jackson ImmunoResearch. Phalloidin-543 was obtained from Sigma (P1951) and Phalloidin-647 from Abcam (ab176759). Images were captured using a Leica SP5 laser confocal microscope.

EdU pulse-chase assay
An EdU pulse-chase assay was performed as described previously (Hu et al., 2018). Pregnant female mice were injected with 500 μg EdU (Invitrogen) at E9.25-9.5 and embryos were harvested 2 h later to detect the labeled cells proliferating during this period. To chase the EdU$^+$ cells, female mice were injected with 5 mg thymidine (Sigma) after the 2-h EdU pulsing period to compete against the incorporation of EdU. Embryos were collected 19 h later at E10.0-10.5. All the embryos were processed for serial paraffin sections, and then stained for EdU according to the manufacturer's recommendation (Invitrogen).

RNA-Seq analysis and RT-qPCR
aDPW and OFT tissues were dissected from control and *Hand2* mutant embryos at E9.0-E9.5 and pooled. Total RNA was extracted from these tissues using Trizol. Three biological replicates for each group (control and *Hand2* deletion, 21 tissues per group) were processed and assessed in the Illumina HiSeq™2500/Miseq sequencing platform (Novogene). The differentially expressed genes were analyzed with DESeq (Novogene). GO enrichment was analyzed via GOseq (Novogene). For RT-qPCR, tissue collection and RNA isolation were performed as described above. Primers used for qPCR analysis are listed in Table S2.

Western blot analysis
OFT tissues microdissected from control and *Hand2* mutant embryos or H9C2 cells collected from normal control (NC) and Hand2 small interfering RNA (siHAND2) groups were used for protein extraction with RIPA (Beyotime Biotechnology, P0013B). Tissue or cell lysates were prepared with RIPA [20 mM Tris, 150 mM NaCl, 10% glycerol, 20 mM glycerophosphate, 1% NP40, 5 mM EDTA, 0.5 mM EGTA, 1 mM Na$_3$VO$_4$, 0.5 mM PMSF, 1 mM benzamidine, 1 mM DTT, 50 mM NaF, 4 M leupeptin (pH 8.0)]. Anti-HAND2 (generated in collaboration with Abcam, b200040; 1:1000), anti-E-cadherin (Bioworld, BS1098; 1:1000), anti-N-cadherin (Abcam, ab98952; 1:1000), anti-STARS (Proteintech, 22673-1-AP; 1:1000) and anti-SRF (Santa Cruz, sc-335; 1:1000) antibodies were used, with anti-β-actin (Bioworld, BS6007M; 1:5000), anti-α-tubulin (Bioworld, BS1699; 1:5000) or anti-GAPDH (Bioworld, AP0063; 1:5000) antibodies as internal controls. Samples were resolved by SDS-PAGE and transferred to PVDF membranes (Millipore). Membranes were

blocked with 5% non-fat milk in TBST [50 mM Tris, 150 mM NaCl, 0.5 mM Tween-20 (pH 7.5)] and then incubated with primary antibodies overnight at 4 °C. Protein levels were quantified using ImageJ software. Each experiment was repeated at least twice.

Plasmid construction for luciferase reporter assay
The full-length fragment of the mouse *Hand2* coding sequence (CDS) was cloned into the pCMV7.1-3×FLAG vector. Two ~1.6 kb and ~0.4 kb fragments, corresponding to the *Stars* 5′ flanking sequence, were amplified via PCR from mouse genomic DNA and cloned into the pGL3-Basic Vector (Promega) to generate a *Stars*-luc vector. The *Stars* mut-luc vector, which contained a 3-bp mutation in the mouse *Stars* E-box (A/T to G), was generated by mutation PCR. The primers used are listed in Table S2. Luciferase reporter assays in HEK293T and H9C2 cells were performed using the Dual Luciferase Assay System (Promega), following a standard protocol. Each assay was repeated three times.

RNAi
For RNAi analysis of *Hand2* in H9C2 cells, a 21-nucleotide small interfering RNA (siRNA) duplex was synthesized as follows: sense: 5′-UCAAGGCGGAGAUCAAGAAUU-3′; antisense: 5′-UUCUUGAU-CUCCGCCUUGATT-3′. siRNA with sense: 5′-UUCUUCGAACGUGU-CACGUTT-3′; antisense: 5′-ACGUGACACGUUCGGAGAAUU-3′ was used as negative control. Transfections were performed using Lipo3000 (Invitrogen) according to the manufacturer's instructions. Cells were used for the luciferase reporter assays or harvested for western blot analysis.

ChIP-qPCR
ChIP assays were performed according to a protocol from Dr Aibin He's lab (Peking University). In brief, H9C2 cells with exogenous mouse HAND2 overexpression were collected and crosslinked with 1% formaldehyde for 10 min at room temperature and subsequently quenched with glycine to a final concentration of 0.125M for another 10 min. Chromatin was sonicated with a Bioruptor (Diagenode), cleared by centrifugation (10 min, 4°C, 15,000 *g*), and incubated overnight at 4°C with 5 μg anti-Flag antibody (Sigma F1804). Immunocomplexes were immobilized with 100 μl protein-G Dynal magnetic beads (Invitrogen) for 4 h at 4°C, followed by stringent washes and elution. Eluates were subject to reversal of crosslinks overnight at 65°C and deproteinated. DNA was extracted with phenol chloroform, followed by ethanol precipitation. ChIP-qPCR analyses were performed using ABI StepOne Plus (ABI). The primers used are shown in Table S2.

Statistical analysis
All data are expressed as mean±s.e.m. Statistical analyses were performed using paired or unpaired *t*-tests as appropriate. Significance of differences was calculated with GraphPad Prism6. *P*-values <0.05 were considered significant.

Data availability
RNA-seq data have been deposited in GEO under accession number GSE131362.

Supplementary information
Supplementary information available online at
http://dev.biologists.org/lookup/doi/10.1242/dev.177477.supplemental

References

Akiko, A., Spencer, J. A. and Olson, E. N. (2002). STARS, a striated muscle activator of Rho signaling and serum response factor-dependent transcription. *J. Biol. Chem.* **277**, 24453-24459. doi:10.1074/jbc.M202216200

Berrier, A. L. and Yamada, K. M. (2010). Cell-matrix adhesion. *J. Cell. Physiol.* **213**, 565-573. doi:10.1002/jcp.21237

Black, B. L. (2007). Transcriptional pathways in second heart field development. *Semin. Cell Dev. Biol.* **18**, 67-76. doi:10.1016/j.semcdb.2007.01.001

Boon-Seng, S., Kristina, B., Huansheng, X., Edward, L., Shi-Yan, N., Hao, W., Jolanta, C., Xin, J., Lei, B. and Li, R. A. (2014). N-cadherin prevents the premature differentiation of anterior heart field progenitors in the pharyngeal mesodermal microenvironment. *Cell Res.* **24**, 1420-1432. doi:10.1038/cr.2014.142

Bruneau, B. G. (2008). The developmental genetics of congenital heart disease. *Nature* **451**, 943-948. doi:10.1038/nature06801

Chong, N. W., Koekemoer, A. L., Ounzain, S., Samani, N. J., Shin, J. T. and Shaw, S. Y. (2012). STARS is essential to maintain cardiac development and function in vivo via a SRF pathway. *PLoS ONE* **7**, e40966. doi:10.1371/journal.pone.0040966

Cortes, C., Francou, A., De, Bono, C. and Kelly, R. G. (2018). Epithelial properties of the second heart field. *Circ. Res.* **122**, 142-154. doi:10.1161/CIRCRESAHA.117.310838

De Soysa, T. Y., Ranade, S., Okawa, S., Ravichandran, S., Huang, Y., Salunga, H. T., Schricker, A., Sol, A. D., Gifford, C. and Srivastava, D. (2018). Single-cell transcriptome analysis during cardiogenesis reveals basis for organ level developmental anomalies. *bioRxiv* doi:10.1101/365734.

Fahed, A. C., Gelb, B. D., Seidman, J. G. and Seidman, C. E. (2013). Genetics of congenital heart disease: the glass half empty. *Circ. Res.* **6**, 707-720. doi:10.1161/CIRCRESAHA.112.300853

Firulli, B. A., Howard, M. J., McDaid, J. R., Mcilreavey, L., Dionne, K. M., Centonze, V. E., Cserjesi, P., Virshup, D. M. and Firulli, A. B. (2003). PKA, PKC, and the protein phosphatase 2A influence HAND factor function: a mechanism for tissue-specific transcriptional regulation. *Mol. Cell* **12**, 1225-1237. doi:10.1016/S1097-2765(03)00425-8

Francou, A., Saint-Michel, E., Mesbah, K. and Kelly, R. G. (2014). TBX1 regulates epithelial polarity and dynamic basal filopodia in the second heart field. *Development* **141**, 4320-4331. doi:10.1242/dev.115022

Gumbiner, B. M. (2005). Regulation of cadherin-mediated adhesion in morphogenesis. *Nat. Rev. Mol. Cell Biol.* **6**, 622-634. doi:10.1038/nrm1699

Harvey, R. P. (2002). Patterning the vertebrate heart. *Nat. Rev. Genet.* **3**, 544. doi:10.1038/nrg843

Holler, K. L., Hendershot, T. J., Troy, S. E., Vincentz, J. W., Firulli, A. B. and Howard, M. J. (2010). Targeted deletion of Hand2 in cardiac neural crest-derived cells influences cardiac gene expression and outflow tract development. *Dev. Biol.* **341**, 291-304. doi:10.1016/j.ydbio.2010.02.001

Hu, J., Shi, Y., Xia, M., Liu, Z., Zhang, R., Luo, H., Zhang, T., Yang, Z. and Yuan, B. (2018). WDR1-regulated actin dynamics is required for outflow tract and right ventricle development. *Dev. Biol.* **438**, 124-137. doi:10.1016/j.ydbio.2018.04.004

Hynes, R. O. (2002). Integrins: bidirectional, allosteric signaling machines. *Cell* **110**, 673-687. doi:10.1016/S0092-8674(02)00971-6

Kalluri, R. and Weinberg, R. A. (2009). The basics of epithelial-mesenchymal transition. *J. Clin. Investig.* **119**, 1420-1428. doi:10.1172/JCI39104

Kelly, R. G., Buckingham, M. E. and Moorman, A. F. (2014). Heart fields and cardiac morphogenesis. *Cold Spring Harb. Perspect Med.* **4**, a015750. doi:10.1101/cshperspect.a015750

Koichiro, K., Barrientos, T., Pipes, G. C. T., Li, S. and Olson, E. N. (2005). Muscle-specific signaling mechanism that links actin dynamics to serum response factor. *Mol. Cell. Biol.* **25**, 3173-3181. doi:10.1128/MCB.25.8.3173-3181.2005

Le, A. T. and Stainier, D. Y. R. (2004). Fibronectin regulates epithelial organization during myocardial migration in Zebrafish. *Dev. Cell* **6**, 371-382. doi:10.1016/S1534-5807(04)00063-2

Li, D., Sinha, T., Ajima, R., Seo, H.-S., Yamaguchi, T. P. and Wang, J. (2016). Spatial regulation of cell cohesion by Wnt5a during second heart field progenitor deployment. *Dev. Biol.* **412**, 18-31. doi:10.1016/j.ydbio.2016.02.017

Luo, W., Zhao, X., Jin, H., Tao, L., Zhu, J., Wang, H., Hemmings, B. A. and Yang, Z. (2015). Akt1 signaling coordinates BMP signaling and β-catenin activity to regulate second heart field progenitor development. *Development* **142**, 732-742. doi:10.1242/dev.119016

Ma, Q., Zhou, B. and Pu, W. T. (2008). Reassessment of Isl1 and Nkx2-5 cardiac fate maps using a Gata4 -based reporter of Cre activity. *Dev. Biol.* **323**, 98-104. doi:10.1016/j.ydbio.2008.08.013

Métais, A., Lamsoul, I., Melet, A., Uttenweiler-joseph, S., Poincloux, R., Stefanovic, S., Valière, A., Gonzalez de Peredo, A., Stella, A. and Burlet-schiltz, O. (2018). Asb2α–Filamin a axis is essential for actin cytoskeleton remodeling during heart development. *Circ. Res.* **122**. doi:10.1161/CIRCRESAHA.117.312015

Nieto, M. A. (2013). Epithelial plasticity: a common theme in embryonic and cancer cells. *Science* **342**, 708. doi:10.1126/science.1234850

Parsons, J. T., Horwitz, A. R. and Schwartz, M. A. (2010). Cell adhesion: integrating cytoskeletal dynamics and cellular tension. *Nat. Rev. Mol. Cell Biol.* **11**, 633. doi:10.1038/nrm2957

Perez-Moreno, M., Jamora, C. and Fuchs, E. (2003). Sticky business: orchestrating cellular signals at Adherens junctions. *Cell* **112**, 535-548. doi:10.1016/S0092-8674(03)00108-9

Prall, O. W. J., Menon, M. K., Solloway, M. J., Watanabe, Y., Zaffran, S., Bajolle, F., Biben, C., Mcbride, J. J., Robertson, B. R. and Chaulet, H. (2007). An Nkx2-5/Bmp2/Smad1 negative feedback loop controls heart progenitor specification and proliferation. *Cell* **128**, 947-959. doi:10.1016/j.cell.2007.01.042

Ramsbottom, S. A., Sharma, V., Rhee, H. J., Eley, L., Phillips, H. M., Rigby, H. F., Dean, C., Chaudhry, B. and Henderson, D. J. (2014). Vangl2-regulated polarisation of second heart field-derived cells is required for outflow tract lengthening during cardiac development. *PLoS Genet.* **10**, e1004871. doi:10.1371/journal.pgen.1004871

Schindler, Y. L., Garske, K. M., Jinhu, W., Firulli, B. A., Firulli, A. B., Poss, K. D. and Deborah, Y. (2014). Hand2 elevates cardiomyocyte production during zebrafish heart development and regeneration. *Development* **141**, 3112-3122. doi:10.1242/dev.106336

Sinha, T., Wang, B., Evans, S., Wynshawboris, A. and Wang, J. (2012). Disheveled mediated planar cell polarity signaling is required in the second heart field lineage for outflow tract morphogenesis. *Dev. Biol.* **370**, 135-144. doi:10.1016/j.ydbio.2012.07.023

Srivastava, D. (2006). Making or breaking the heart: from lineage determination to morphogenesis. *Cell* **126**, 1037-1048. doi:10.1016/j.cell.2006.09.003

Srivastava, D. and Olson, E. N. (2000). A genetic blueprint for cardiac development. *Nature* **407**, 221-226. doi:10.1038/35025190

Srivastava, D., Thomas, T., Lin, Q., Kirby, M. L., Brown, D. and Olson, E. N. (1997). Regulation of cardiac mesodermal and neural crest development by the bHLH transcription factor, dHAND. *Nat. Genet.* **16**, 154-160. doi:10.1038/ng0697-154

Takeichi, M. (2014). Dynamic contacts: rearranging adherens junctions to drive epithelial remodelling. *Nat. Rev. Mol. Cell Biol.* **15**, 397-410. doi:10.1038/nrm3802

Thiery, J. P. (2003). Cell adhesion in development: a complex signaling network. *Curr. Opin. Genet. Dev.* **13**, 365-371. doi:10.1016/S0959-437X(03)00088-1

Tsuchihashi, T., Maeda, J., Shin, C. H., Ivey, K. N., Black, B. L., Olson, E. N., Yamagishi, H. and Srivastava, D. (2011). Hand2 function in second heart field progenitors is essential for cardiogenesis. *Dev. Biol.* **351**, 62-69. doi:10.1016/j.ydbio.2010.12.023

VanDusen, N., Casanovas, J., Vincentz, J. W., Firulli, B. A., Osterwalder, M., Lopez-Rios, J., Zeller, R., Zhou, B., Grego-Bessa, J. and Delapompa, J. (2014). Hand2 is an essential regulator for two notch-dependent functions within the embryonic endocardium. *Cell Rep.* **9**, 2071-2083. doi:10.1016/j.celrep.2014.11.021

Verzi, M. P., McCulley, D. J., De Val, S., Dodou, E. and Black, B. L. (2005). The right ventricle, outflow tract, and ventricular septum comprise a restricted expression domain within the secondary/anterior heart field. *Dev. Biol.* **287**, 134-145. doi:10.1016/j.ydbio.2005.08.041

Vincent, S. D. and Buckingham, M. E. (2010). How to make a heart: the origin and regulation of cardiac progenitor cells. *Curr. Top. Dev. Biol.* **90**, 1-41. doi:10.1016/S0070-2153(10)90001-X

Vincentz, J. W., Barnes, R. M. and Firulli, A. B. (2011). Hand factors as regulators of cardiac morphogenesis and implications for congenital heart defects. *Birth Defects Res. A Clin. Mol. Teratol.* **91**, 485-494. doi:10.1002/bdra.20796

Wolpert, L., Jessell, T., Lawrence, P., Meyerowitz, E., Robertson, E. and Smith, J. (2006). *Principles of Development*, 3rd edn. Oxford University Press.

Xiao, Q., Zhang, G., Wang, H., Chen, L., Lu, S., Pan, D., Liu, G. and Yang, Z. (2017). A p53-based genetic tracing system to follow postnatal cardiomyocyte expansion in heart regeneration. *Development* **144**, 580-589. doi:10.1242/dev.147827

Yamagishi, H., Olson, E. N. and Srivastava, D. (2000). The basic helix-loop-helix transcription factor, dHAND, is required for vascular development. *J. Clin. Investig.* **105**, 261-270. doi:10.1172/JCI8856